# Multiple trapping sites and symmetry splitting in cryogenic matrices: Infrared spectroscopy of HCN in Ar, Kr, and Xe

Alison D. Abbate and C. Bradley Moore

Citation: The Journal of Chemical Physics **82**, 1255 (1985); doi: 10.1063/1.448446
View online: http://dx.doi.org/10.1063/1.448446
View Table of Contents: http://scitation.aip.org/content/aip/journal/jcp/82/3?ver=pdfcov
Published by the AIP Publishing

# Multiple trapping sites and symmetry splitting in cryogenic matrices: Infrared spectroscopy of HCN in Ar, Kr, and Xe

Alison D. Abbate[a] and C. Bradley Moore
*Department of Chemistry, University of California, Berkeley, California 94720*

(Received 12 March 1984; accepted 19 October 1984)

Infrared spectra of $HC^{14}N$ and $HC^{15}N$ trapped in cryogenic matrices of Ar, Kr, and Xe and of DCN in Xe have been measured. In addition to the fundamental frequencies, overtone and combination bands along with their anharmonic constants are reported. In the Kr and Xe matrices several of the bands exhibit multiple peaks. Changes in the bands with temperature, concentration, annealing, and host indicate that there are two trapping sites. In Xe the degeneracy of the C–H bend $\nu_2$ is split in one site. The spectral data in Xe may be understood in terms of HCN in a substitutional site of the face-centered-cubic rare gas lattice with some molecules oriented along the $\langle 111 \rangle$ axis and others along the $\langle 110 \rangle$ axis. The low symmetry about the $\langle 110 \rangle$ axis removes the degeneracy between the two bending coordinates of an HCN oriented along it. Two sites occur in Kr. Although a splitting of the $\nu_2$ degeneracy is not resolved, the same sites are probably involved in both Kr and Xe. A single unsplit site is observed for Ar.

## I. INTRODUCTION

A spectroscopic study of HCN isolated in Ar, Kr, and Xe matrices was undertaken to provide the basic data for vibrational energy transfer experiments. Spectra of HCN in cryogenic matrices have been reported previously. King and Nixon[1] measured spectra of the fundamental bands of HCN in Ar, $N_2$, and CO matrices, and of DCN in Ar and $N_2$ matrices. Through the concentration and diffusion dependence of the spectra they identified monomer, dimer, and polymer bands. Pacansky and Calder[2,3] reported the fundamental frequencies of six isotopes of HCN in Ar matrices. In addition to the fundamental frequencies, the present work provides the combination and overtone frequencies of $HC^{14}N$ and $HC^{15}N$ in Ar and the first reported spectra of $HC^{14}N$ and $HC^{15}N$ in Kr and Xe, and of DCN in Xe.

The existence of multiple trapping sites in matrices has been elegantly demonstrated through site-specific, laser-induced isomerization of $Fe(CO)_4$ by Davies *et al.*[4,5] Pimentel *et al.*[6] presented the first evidence that the matrix lattice can split the degenerate vibrations of a trapped species. They found that the linewidths of the symmetric bands of $NH_3$ in $N_2$ matrices were distinctly narrower than those of the degenerate $E$ modes and attributed this broadening to degeneracy splitting. A single site with symmetry splitting was proposed by King and Nixon[1] for HCN in $N_2$ and CO matrices. They observed two peaks for the degenerate bend $\nu_2$ and single peaks for $\nu_1$ and $\nu_3$. More recently, Swanson and Jones[7,8] have invoked site symmetry splittings to explain the complicated spectra of the $\nu_3$ mode of $SF_6$ and $SeF_6$ in Ar and Kr matrices.

The spectra of HCN in Xe and Kr and of DCN in Xe provide strong evidence for the existence of two trapping sites, one in which the bending degeneracy is retained and another in which it is split. The two sites are assigned as HCN oriented along the $\langle 1\,1\,1 \rangle$ or $\langle 1\,1\,0 \rangle$ axes, respectively, of a substitutional site.

## II. EXPERIMENTAL

Matrix mixtures were prepared in the gas phase in a greased glass high vacuum line with a Hg diffusion pump. For DCN matrices the line was deuterated by at least five 30 min exposures to 5 Torr $D_2O$, between which the line was pumped to $1 \times 10^{-5}$ Torr. A triple McLeod gauge and a Hg manometer measured the pressure. To avoid HCN dissolving in the grease, mixing times were between 2–5 h. Mixing was expedited by rapidly admitting the rare gas to a 12 $l$ bulb which contained a measured amount of HCN. Matrix concentrations were assumed to be the same as in the gas phase. The number of moles in the matrix was calculated from the decrease in gas pressure during deposition.

Matrices were deposited onto a CsI substrate in an Air Products Inc. Model CSA 202 displex. The temperature was determined by an $H_2$ thermometer or by a KP vs Au 0.07 at. % Fe thermocouple referenced in ice water. The temperature was stable at 9.0 ± 0.3 K at the minimum temperature. At a typical temperature for experiments, 25 K, a stability of ±0.1 K was obtained.

Pulsed deposition was chosen because it allows fast deposition rates with good isolation, thereby producing high purity matrices. The spray-on nozzle was a 4.5 mm i.d. stainless steel tube normal to the substrate at a distance of 1.9 cm. Four pulses per min (12 ml, 40–120 Torr) gave a deposition rate of 18 mmol/h. Because HCN

[a] Present address: Solar Energy Research Institute, 1617 Cole Boulevard, Golden, CO 80401.

 0021-9606/85/031255-08$02.10  

is polar it tends to aggregate during deposition. The degree of isolation depended on the concentration and deposition temperature but was insensitive to the pulse size over the above pressure range. Although Xe matrices are generally deposited at 25 K to improve the crystal structure and hence decrease light scattering, in this work a 9 K substrate for all rare gases was required to prevent aggregate formation. Some matrices were annealed by warming to 40 K for < 5 min and cooling to 9 K in 20 min.

The matrices were characterized with infrared spectroscopy using a Nicolet 7199 FTIR equipped with either a cooled HgCdTe detector or a cooled Insb/HgCdTe sandwich detector. Since most of the experiments used highly scattering Xe matrices, it was typically necessary to average 5000 scans. For most of the spectra, a resolution of 0.5 $cm^{-1}$ was chosen as a compromise between low noise and high resolution. Spectra in each host were recorded with 0.24 $cm^{-1}$ resolution to determine the linewidths. The narrowest linewidths were 0.5 $cm^{-1}$.

The fraction of HCN dimers was approximated from the $\nu_3$ absorption by assuming equal oscillator strengths for the monomer and non-H-bonded dimer. Impurities from leaks during deposition could be measured from the matrix $H_2O$ absorption at 1630 $cm^{-1}$. To determine the percent deuteration of the DCN matrices the integrated absorptions of the $\nu_3$ bands were compared. For the two DCN/Xe matrices, the DCN:HCN absorbance ratios were 3.3 and 5.5. Kim and King[9] give the ratio of gas phase HCN to DCN line strengths as 2.0. Therefore the matrices were 87% and 92% deuterated.

HCN was synthesized by adding dilute $H_2SO_4$ (Mallinckrodt AR) to NaCN (Mallinckrodt >95%). The product was distilled two times from 195 to 77 K. For $HC^{15}N$ the starting material was $KC^{15}N$ (Stohler Isotope Chemicals 99% $^{15}N$). DCN was synthesized with DCl (Aldrich >99% D, 20% DCl in $D_2O$). The isotopic purity of the product was >95% when the vacuum system was carefully deuterated. The matrix gases used were Ar (Matheson 99.9995%), Kr (Airco 99.995%), and Xe (Airco 99.995%).

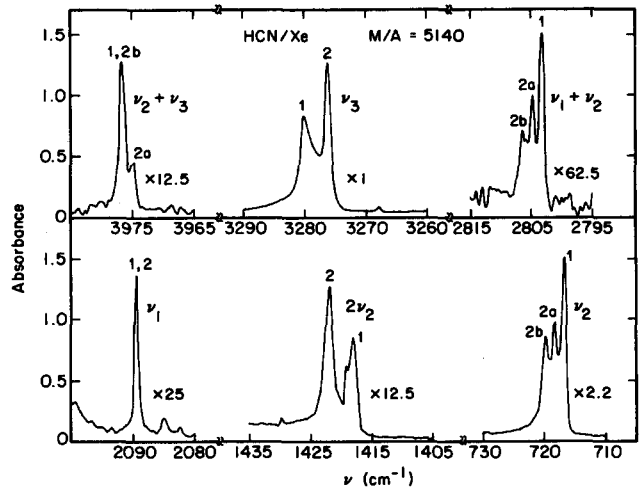


FIG. 2. All routinely observable bands of HCN/Xe at 9 K. Divide the absorbance scale by the multiplier for each band. Bands are labeled as site-1 or site-2. Deposition conditions were $T$ = 9 K, $M/A$ = 5140, 15.9 mmol.

The Kr and Xe were subjected to two freeze–pump–thaw cycles at 77 K.

## III. RESULTS AND DISCUSSION

Figure 1 shows spectra of the HCN C–H stretch $\nu_3$ and of the fundamental and first overtone of the C–H bend, $\nu_2$ and $2\nu_2$, in Ar and Kr matrices. Figure 2 shows a complete set of the observed spectral lines for HCN in Xe. DCN in Xe (Fig. 3) looks qualitatively like HCN except that two peaks are resolved for $\nu_1$.

The interaction of the HCN molecule with its rare gas environment shifts the absorption frequencies from their gas phase values. Table I shows the absorption frequencies for HCN gas[10] and for HCN in Ar, Kr, and Xe. The frequencies for $HC^{15}N$ and DCN are also listed. The matrix frequencies are reproducible to ±0.2 $cm^{-1}$. The C–H bend $\nu_2$ is blue shifted from the gas phase while the C–H stretch $\nu_3$ is red shifted. The C–N stretch $\nu_1$

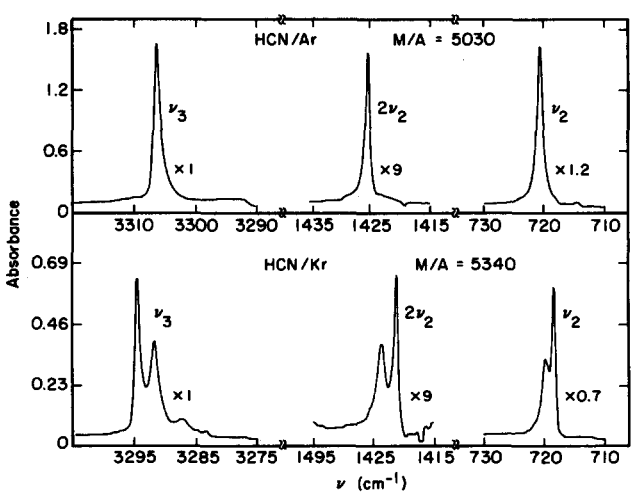


FIG. 1. Spectra of the C–H stretch and bend in HCN/Ar and HCN/Kr at 9 K. The absorbance scale, $\log_{10}(I/I_0)$, should be divided by the multiplier for each band. Matrices were deposited at 9 K. The Ar matrix has $M/A$ = 5030, 30.4 mmol, Kr has $M/A$ = 5340, 16.6 mmol.

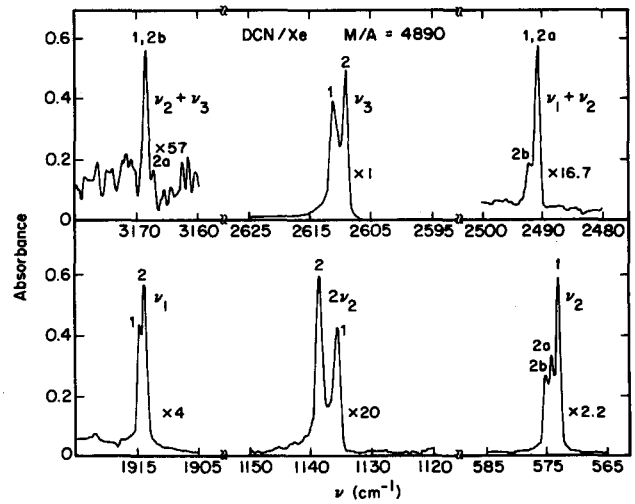


FIG. 3. DCN/Xe matrix at 9 K. Divide absorbance scale by multiplier for each band. Peaks have been assigned to site-1 or site-2. The $\nu_1$ band has two peaks, compared to one in HCN. Deposition conditions were $T$ = 9 K, $M/A$ = 4890, 14.8 mmol, 87% deuterated.

TABLE I. Absorption frequencies ($cm^{-1}$) of HCN in matrices.

| | $HC^{14}N$ | | | | $HC^{15}N$ | | | | $DC^{14}N$ | |
|---|---|---|---|---|---|---|---|---|---|---|
| Band | gas[a] | Ar | Kr | Xe | gas[b] | Ar | Kr | Xe | gas[b] | Xe |
| $(01^10)$ | 711.98 | 720.9 | 718.6 | 716.7 | 712.46 | 719.8 | 717.6 | 715.7 | 570.25 | 573.2 |
| | | | 719.9 | 718.4 | | | 719.2 | 717.4 | | 574.3 |
| | | | | 719.8 | | | | 718.7 | | 575.2 |
| $(02^00)$ | 1411.43 | 1425.4 | 1421.4 | 1417.9 | | 1423.7 | 1420.6 | 1416.0 | | 1135.7 |
| | | | 1423.8 | 1422.0 | | | [c] | 1419.4 | | 1138.8 |
| $(03^10)$ | | | | 2124.7 | | | | | | |
| | | | | 2129.1 | | | | | | |
| $(10^00)$ | 2096.85 | 2097.7 | 2094.1 | 2089.5 | 2064.35 | 2065.4 | 2059.7 | 2057.2 | 1925.24 | 1914.0 |
| | | | | | | | | | | 1914.8 |
| $(11^10)$ | 2805.58 | 2815.3 | 2809.6 | 2803.4 | | 2782.0 | 2774.4 | 2770.1 | | 2491.0 |
| | | | 2810.9 | 2805.0 | | | 2775.4 | 2771.8 | | 2492.4 |
| | | | | 2806.5 | | | | 2773.1 | | |
| $(00^01)$ | 3311.48 | 3306.4 | 3292.0 | 3276.2 | 3310.13 | 3305.0 | 3287.0 | 3274.9 | 2630.34 | 2609.3 |
| | | | 3294.8 | 3280.0 | | | [c] | 3278.5 | | 2611.5 |
| $(01^11)$ | 4004.17 | 4007.6 | 3991.5 | 3974.9 | | 4005.2 | 3986.0 | 3972.5 | | 3167.4 |
| | | | 3993.3 | 3976.9 | | | [c] | 3974.5 | | 3168.8 |

[a] Reference 10 (Nakagawa and Morino).
[b] Reference 3 (Pacanski and Calder).
[c] Only 0.5 $cm^{-1}$ resolution spectra were recorded for these bands and, while two peaks are expected, only one peak could be resolved.

which is allowed but is too weak to observe in the gas phase,[11] is sufficiently perturbed by the matrix that it is easily seen in these spectra. Like the C–H stretch, it is red shifted.

### A. Multiple peaks

The most striking feature of the spectra is the multiple peaks observed for some of the modes. In Ar each band has only one peak which can be distinguished with 0.24 $cm^{-1}$ resolution. In the larger cages of Kr and Xe crystals, many bands have two or three peaks. Multiple peaks in the absorption bands of trapped species may be caused by (i) aggregate formation, (ii) guest rotation, (iii) multiple trapping sites, or (iv) the splitting of a degeneracy.

#### 1. Dimers: Concentration dependence

Concentration and diffusion studies can distinguish among peaks due to monomers, dimers, and higher order polymers. Spectra of a relatively concentrated HCN/Xe matrix (Fig. 4) show the growth of two dimer absorptions for each of the fundamentals. This agrees with King and Nixon's study of HCN dimer in Ar[1] which indicates a linear hydrogen-bonded HCN–HCN dimer. For each fundamental there is one dimer absorption which is close to the fundamental in frequency and a hydrogen-bonded band which is shifted by as much as 84 $cm^{-1}$. Dimerization changes the accidentally small matrix element of the C–N stretch so that the intensity of the dimer $\nu_1$ absorption is increased relative to that of the monomer. These concentration studies show that the multiple peaks in Figs. 1–3 are not due to HCN dimer.

#### 2. Rotation: Temperature dependence

Several small molecules, notably hydrogen halides[12] rotate in matrix cages. It is tempting to suggest that HCN might rotate in Xe since the parallel $\nu_3$ and $2\nu_2$ bands have two peaks, presumably the $P$ and $R$ envelopes, while

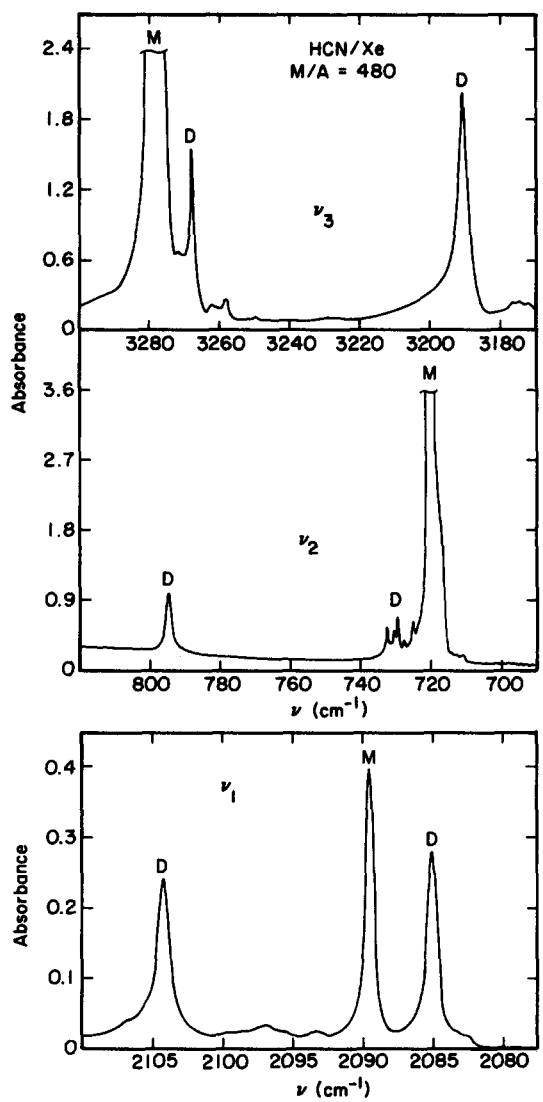


FIG. 4. Dimer bands for HCN/Xe at $M/A$ = 480. Each transition has one dimer band which is close to the monomer in frequency and an H-bonded one which is shifted more. For $\nu_1$ the absorption strength is larger for the dimer than for the monomer. Deposition conditions were $T$ = 9 K, $M/A$ = 480, 16.9 mmol.

the perpendicular $\nu_2$ and $\nu_1 + \nu_2$ bands have three peaks. The third would be assigned to the $Q$ branch. For restricted rotation the lines should be separated by less than the $2B = 2.95$ cm$^{-1}$ of gas phase HCN.[13] The observed spacings are about 1.5 cm$^{-1}$ for the three $\nu_2$ lines but about 4 cm$^{-1}$ for the pairs of $2\nu_2$ and $\nu_3$ bands, a bit too large. If HCN were rotating, the band intensities would show a strong temperature dependence. The $\nu_2$ and $\nu_3$ bands change reversibly with temperature (Fig. 5). If the temperature is not raised above 30 K, the spectrum upon cooling to 9 K is not noticeably changed. The bands broaden with temperature but do not change significantly in frequency or integrated intensity. The spectra in Fig. 5 are not at all consistent with the intensity changes which would be produced by a rotating molecule with $B \sim 1.5$ cm$^{-1}$.

### 3. Multiple sites: Annealing effect

When the matrix is annealed to 40 K, there are irreversible changes in the relative intensities of the bands (Fig. 6). The bands which increase in intensity are not at the frequency of the dimer absorptions shown in Fig. 4. This indicates that they are due to multiple trapping sites for the monomer and that the matrix rearranges with annealing to increase the number of HCN molecules in the more stable trapping site. Those bands which increase in relative intensity with annealing are assigned to site-1 and those which decrease are assigned to site-2. These assignments are labeled in Fig. 2. It is interesting that the higher energy peak of $\nu_3$ correlates with the lowest energy peaks of $\nu_2$ and $2\nu_2$. Both sites have the same $\nu_1$ frequency within the 0.5 cm$^{-1}$ linewidth.

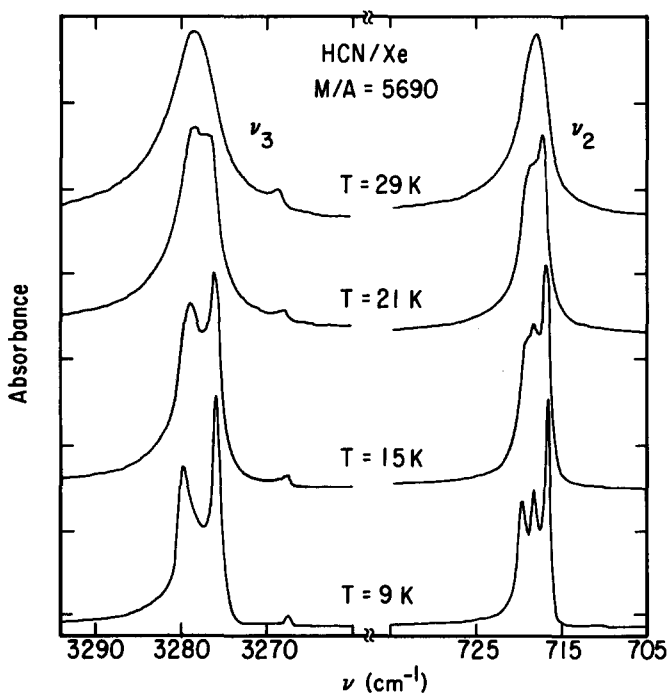


FIG. 5. Reversible broadening of HCN/Xe bands with increased temperature. See Fig. 2 for intensity of $\nu_3$ vs $\nu_2$. The multiple peaks broaden with temperature but do not change in frequency or relative intensity. Deposition conditions were $T = 9$ K, $M/A = 5690$, 17.6 mmol. The 15 K spectra are from a matrix deposited at 9 K, $M/A = 5140$, 15.9 mmol. The spectra have been normalized so that the 9 K spectra for each matrix have the same absorbance.

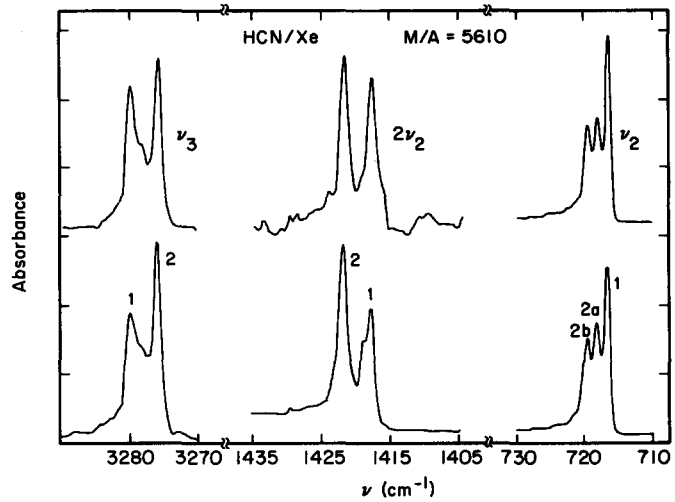


FIG. 6. Irreversible changes with annealing to 40 K for HCN/Xe. The relative intensities of these bands are shown in Fig. 2. The bottom spectrum was deposited at 9 K, $M/A = 5610$, 16.9 mmol. The upper spectrum is the same matrix annealed to 40 K and cooled to 9 K. Intensity changes allow assignment of site-1, which increases relative to site-2.

### 4. Symmetry splitting

It is puzzling that the C–H bend has three peaks while both the overtone of the bend and the C–H stretch have only two. The changes in band intensity with annealing show that there are at least two trapping sites. Each of the three $\nu_2$ bands could be caused by a different site, two of which happen to have the same C–H stretching frequency. The $\chi_{22}$ anharmonicities would have to be different for the sites so that two of them would be coincident in the $\nu_2$ overtone.

A second possibility is a model with only two sites, one of which has lower symmetry and splits the degeneracy of the bend. Loss of cylindrical symmetry means that the vibrational angular momentum about the molecular axis is not a good quantum number and the $l = \pm 1$ degeneracy is split. Both the $\nu_2$ overtone and $\nu_3$ have $l = 0$ and are nondegenerate so they would exhibit only one peak for each site. King and Nixon[1] observed that for HCN and DCN in $N_2$ matrices the $\nu_2$ band is a doublet while the $\nu_1$ and $\nu_3$ bands have single peaks. They proposed a single trapping site which splits the degenerate bend, but did not suggest a structure for the trapping site.

## B. Combination band assignments

### 1. HCN

The assignments of two sites from the annealing studies agree well with the positions and intensities of the combination bands. Using the fundamental frequencies and the relation

$$\omega(1, 1^1, 0) = \omega(1, 0^0, 0) + \omega(0, 1^1, 0) + \chi_{12} \qquad (1)$$

the three $(1, 1^1, 0)$ peaks can all be fit using the same anharmonicity, $\chi_{12} = -2.8 \pm 0.2$ cm$^{-1}$. Similarly, the

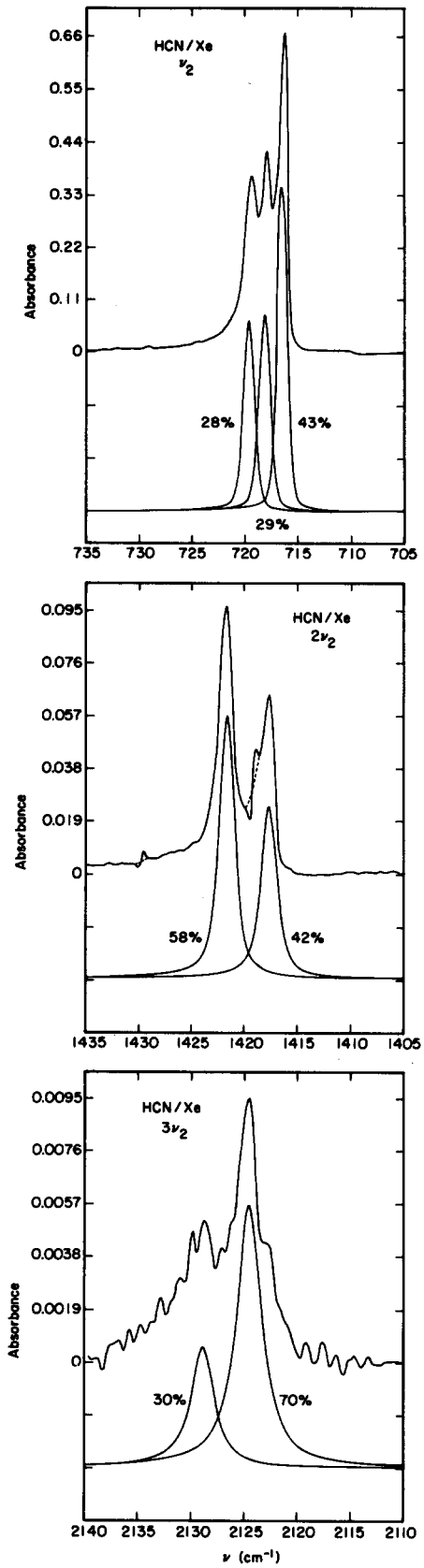


FIG. 7. The $\nu_2$ fundamental and overtones in HCN/Xe at 9 K. The bands have been curve fit with a mixture of Gaussian and Lorentzian line shapes: $\nu_2$ is 60% Gaussian, $2\nu_2$ is 20% Gaussian, $3\nu_2$ is 0% Gaussian. The wings of the spectra could not be fit with substantially different mixtures of line shape functions. Fractional areas are shown for each peak. Broken lines remove atmospheric $H_2O$ background. Deposition conditions for $\nu_2$ and $2\nu_2$ spectra were $T$ = 9 K, $M/A$ = 5140, 15.9 mmol. For $3\nu_2$ they were $T$ = 9 K, $M/A$ = 500, 27.9 mmol.

(0, $1^1$, 1) frequencies in Table I can be fit using $\chi_{23}$ = $-19.8 \pm 0.6$ cm$^{-1}$ for all the peaks. The gas phase values are $-3.6$ and $-19.0$ cm$^{-1}$, respectively.[10] For (0, $1^1$, 1) the combination of the site-1 bands is coincident with the combination of site-2 $\nu_3$ with site-2b $\nu_2$. The weaker (0, $1^1$, 1) line is from site-2 $\nu_3$ combined with site-2a $\nu_2$. Thus the combination of $\nu_3$, which has two lines, with the three lines of $\nu_2$ gives one predominant line and one smaller one in (0, $1^1$, 1).

### 2. DCN

The assignment of the DCN/Xe peaks to site-1 and site-2 is indicated on Fig. 3. For the heavier isotope the $\nu_1$ mode is not exclusively a C–N stretch. Due to its partial C–D character it exhibits two peaks in the spectrum and its intensity is increased relative to that of $\nu_1$ in HCN. This assignment of peaks to site-1 and site-2 gives the correct frequencies and intensities for the combination bands. The shape of the (0, $1^1$, 1) combination band comes from the same type of overlap as in HCN but with $\chi_{23}$ = $-15.9 \pm 0.3$ cm$^{-1}$. For (1, $1^1$, 0) the dominant peak contains both the combination of the site-1 $\nu_2$ and $\nu_1$ bands, and the combination of site-2 $\nu_1$ with site-2a $\nu_2$. The smaller (1, $1^1$, 0) peak is from the sum of site-2 $\nu_1$ and site-2b $\nu_2$. For all three of these the anharmonicity is $\chi_{12}$ = $3.0 \pm 0.3$ cm$^{-1}$. The gas phase values are $\chi_{12}$ = 3.0 cm$^{-1}$ and $\chi_{23}$ = $-15.8$ cm$^{-1}$.[10]

## C. $\nu_2$ overtones

### 1. HCN

Since the $\nu_2$ fundamental has three peaks and the $\nu_2$ overtone has only two, the spectrum of the second overtone should help distinguish between two sites, one of which has a site symmetry splitting, and three sites. The second overtone is a weak band and is not ordinarily observable. A concentrated HCN/Xe matrix with $M/A$ = 500 and a total of 27.9 mmol was deposited to look for $3\nu_2$. The InSb half of the sandwich detector was used and the FTIR was realigned to maximize signal in the 2100 cm$^{-1}$ region. The gain in this spectral region was increased by using low and high pass electronic filters to reduce the signal from other frequencies. Electronic filtering of the interferogram is equivalent to optical filtering of the light source. After averaging 42 000 scans (36 h), the spectrum in Fig. 7 was obtained. The "noise" was reproducible in each set of 7000 scans and therefore could not be reduced by averaging. The same noise appears in the background spectrum but could not be subtracted completely. The spacing of the noise is consistent with interference fringes from a 3 mm thick element, such as a cell or detector window, in the optical path.[14]

The second overtone, like the first, has two absorption peaks. The spectra in Fig. 7 were curve fit[14] using a combination of Lorentzian and Gaussian shapes to determine the areas under the various peaks. The sum of the fractional areas of the two highest frequency $\nu_2$ peaks equals the fractional area of the higher $2\nu_2$ peak, but is larger than the fractional area in the higher $3\nu_2$ peak.

This indicates that the lower energy $3\nu_2$ peak corresponds to two of the $\nu_2$ peaks.

The $\nu_2$ energy levels of a linear triatomic in the gas phase can be described by[15]

$$E/hc = G(v) - G(0) = G_0(v), \tag{2}$$

where

$$G(v) = \omega_2(v_2 + 1) + \chi_{22}(v_2 + 1)^2 + g_{22}l_2^2 \tag{3}$$

and thus

$$G_0(v) = \omega_2^0 v_2 + \chi_{22}v_2^2 + g_{22}l_2^2 \tag{4}$$

with

$$\omega_2^0 = \omega_2 + 2\chi_{22}. \tag{5}$$

From Fig. 7, site-1 can unambiguously be assigned to the lowest energy peak in each of the $\nu_2$ levels. The higher energy $2\nu_2$ peak is too large to be just the site-1 peak but too small to also contain a site-2 peak. The higher energy $3\nu_2$ peak is too small to correspond to site-1. Given these three frequencies it is possible to calculate $\omega_2^0$, $\chi_{22}$, and $g_{22}$.

For the other site or sites there are three possible assignments of the bands. For all assignments both higher frequency $\nu_2$ bands, labeled 2a and 2b in Fig. 2, correlate with the high frequency $2\nu_2$ band. This assignment must be correct for two reasons: the annealing studies identified these bands as belonging to the same site since they all decrease in intensity upon annealing, and the area of the lower energy $2\nu_2$ peak is too small to correlate with two of the $\nu_2$ peaks but too large to be either of the site-2 peaks alone. If three sites are assumed, the middle $\nu_2$ band, labeled 2a, can correlate with either (1) the high frequency $3\nu_2$ band or (2) the lower frequency one, which overlaps the site-1 $3\nu_2$ band. The highest energy $\nu_2$ band, labeled 2b, then correlates to the other $3\nu_2$ band. The third possibility is to assume that the $l = \pm 1$ levels are split in $\nu_2$ and $3\nu_2$ for one of two sites. For states with $l$-type doubling the two component levels are shifted above and below the "original" level by equal amounts.[16] Thus the spectral constants for case 3 were calculated by using the average of the split energies as the unperturbed energy. Table II contains the spectral constants for these three assignments. They will be discussed in Sec. III D.

### 2. DCN

Since the $\nu_2$ oscillator strength is reduced with deuteration, it was not possible to record a $3\nu_2$ spectrum for DCN/Xe. The $\nu_2$ spectral constants must be calculated from those found for HCN/Xe. For most molecules the anharmonic coefficients of the isotopes follow Dennison's Rule[17]

$$\frac{\chi_{ik}^{(i)}}{\chi_{ik}} = \frac{\omega_i^{(i)}\omega_k^{(i)}}{\omega_i\omega_k}. \tag{6}$$

However, for DCN this relation is not followed, particularly not by $\chi_{12}$ which changes sign on deuteration. Instead the DCN/Xe constants were calculated by assuming that the isotopic change is the same in the matrix as in the gas:

$$\left[\frac{\chi_{ik}^{(\mathrm{DCN})}}{\chi_{ik}^{(\mathrm{HCN})}}\right]_{\mathrm{gas}} = \left[\frac{\chi_{ik}^{(\mathrm{DCN})}}{\chi_{ik}^{(\mathrm{HCN})}}\right]_{\mathrm{matrix}}. \tag{7}$$

The equivalent equation was used to obtain $g_{22}$.

The gas phase values of Nakagawa and Morino[10] give $\chi_{22}(\mathrm{DCN})/\chi_{22}(\mathrm{HCN}) = 0.853 \pm 0.075$ and $g_{22}(\mathrm{DCN})/g_{22}(\mathrm{HCN}) = 0.615 \pm 0.120$. DCN/Xe energy levels calculated with these values give perfect agreement with the $\nu_2$ and $2\nu_2$ spectral frequencies for site-1 and are within 1 $\mathrm{cm}^{-1}$ of the observed spectrum for all three possible site-2, 3 assignments, as defined for HCN in Table II. The ratios 0.8 and 0.6 give 0.5 $\mathrm{cm}^{-1}$ agreement with the observed $\nu_2$ and $2\nu_2$ DCN/Xe bands for all site assignments. The latter ratios were used to calculate the anharmonic

TABLE II. Spectroscopic constants ($\mathrm{cm}^{-1}$) for HCN/Xe in different trapping sites.[a]

| | | | Case 1[d] | | Case 2[d] | | Case 3[e] |
|---|---|---|---|---|---|---|---|
| | Gas[b] | Site-1[c] | Site-2 | Site-3 | Site-2 | Site-3 | Site-2 |
| $\nu_{01^10}$ | 711.98 | 716.7 | 718.4 | 719.8 | 718.4 | 719.8 | 719.1 |
| $\nu_{02^00}$ | 1411.43 | 1417.9 | 1422.0 | 1422.0 | 1422.0 | 1422.0 | 1422.0 |
| $\nu_{03^10}$ | 2113.46 | 2124.7 | 2129.1 | 2124.7 | 2124.7 | 2129.1 | 2126.9 |
| $\omega_2^0$ | 709.07 | 713.9 | 716.7 | 719.6 | 718.9 | 717.4 | 718.1 |
| $\chi_{22}$ | −2.44 | −2.48 | −2.83 | −4.28 | −3.93 | −3.17 | −3.55 |
| $g_{22}$ | 5.35 | 5.27 | 4.58 | 4.52 | 3.48 | 5.63 | 4.55 |
| $\chi_{12}$ | −3.61 | −2.8 | −2.8 | −2.8 | −2.8 | −2.8 | −2.8 |
| $\chi_{23}$ | −18.98 | −19.8 | −19.8 | −19.8 | −19.8 | −19.8 | −19.8 |

[a] Constants are defined in Eq. (4).
[b] Reference 10.
[c] The site-1 values hold for all three assignments of the other peaks.
[d] Assignments 1 and 2 are based on the assumption that there are three sites, two of which are accidentally degenerate for (0, $2^0$, 0) and (0, $3^1$, 0).
[e] Assignment 3 is based on the assumption that the $\nu_2$ levels of site-2 are split when $l \neq 0$. For the levels which are split, the average of the split frequencies is used to calculate the spectral constants.

constants. For site-1, $\omega_2^0 = 572.0\ cm^{-1}$, $\chi_{22} = -1.98\ cm^{-1}$, and $g_{22} = 3.16\ cm^{-1}$.

### D. Trapping sites

#### 1. Anharmonic constants

The changes in line intensity with annealing (Fig. 6) show that there are at least two different trapping sites. The assignments of the combination bands support the identification of two types of sites. The anharmonic constants in Table II can help determine if each of the three $\nu_2$ peaks is due to a separate site or if there are only two sites, one of which splits the $\nu_2$ degeneracy.

The $\nu_2$ constants for HCN/Xe in site-1 are within 2% of the gas phase values. For any of the three assignments of the site-2, 3 peaks the constants differ from those in the gas phase. Consider first the possibility of three trapping sites. In this case site-2 and site-3 have the same frequency for both the $\nu_3$ and $\nu_1$ stretches. This suggests that they are very similar trapping sites. However, for the case 1 assignment (Table II) the $\chi_{22}$ values of site-2 and site-3 differ by 50%. For the case 2 assignment, the $g_{22}$ values differ by more than 50%. Either of these seems unlikely. For the third case, in which site-2 splits the $\nu_2$ degeneracy, $\chi_{22}$ is more negative than the gas phase value by 45% and $g_{22}$ is decreased by 15%. Since the matrix must perturb the molecule sufficiently to split the degeneracy, it is reasonable that the $\nu_2$ spectral constants should also be affected. Therefore, while the anharmonic constants do not definitively distinguish between the two and three site models, they are more reasonable for the two-site case 3 than for either of the three-site possibilities, cases 1 or 2.

#### 2. Physical model

While multiple trapping sites have often been proposed to rationalize multiple peaks in absorption spectra of matrix isolated molecules, there have been no structural explanations of these trapping sites. To see how HCN fits into a matrix cage, the size of the HCN molecule is estimated by adding the bond lengths[18] to the H and N radii. The radius of H is taken as half the Lennard-Jones diameter for $CH_4$[19] minus the C–H bond length in $CH_4$.[20] This gives 0.81 Å. The radius of N is taken as half the Lennard-Jones diameter for $N_2$[19] minus half the N–N bond length in $N_2$.[21] This gives 1.30 Å. HCN is then 4.33 Å long. Ar, Kr, and Xe form face centered cubic lattices with substitutional site spherical cavity diameters of 3.76, 4.00, and 4.34 Å.[22] Thus HCN is a tight fit in a substitutional site for Ar and Kr matrices and in all rare gases the host atoms will probably distort around the HCN. The C–N stretch has a single peak while the C–H bend and stretch have multiple peaks. This suggests that the C and N are more within the lattice vacancy while the H fills interstices in the surrounding lattice in different positions.

For HCN in a substitutional site there are four orientations (Figs. 8 and 9) which correspond to potential energy minima or maxima. The hydrogen atom may point directly at a nearest neighbor atom ($\langle 1\,1\,0\rangle$), or it may point between two ($\langle 1\,1\,2\rangle$), three ($\langle 1\,1\,1\rangle$), or four ($\langle 1\,0\,0\rangle$) nearest neighbors. The $\langle 1\,1\,0\rangle$ and $\langle 1\,1\,2\rangle$ axes are $C_2$ and thus the $\nu_2$ degeneracy is broken for the first two orientations. (There are no degenerate representations for $C_2$.) They are candidates for site-2. The $\langle 1\,1\,1\rangle$ and $\langle 1\,0\,0\rangle$ are $C_3$ and $C_4$, respectively, and leave the bending degeneracy unbroken ($x$ and $y$ are a basis for the twofold degenerate $E$ representation). These orientations are candidates for site-1.

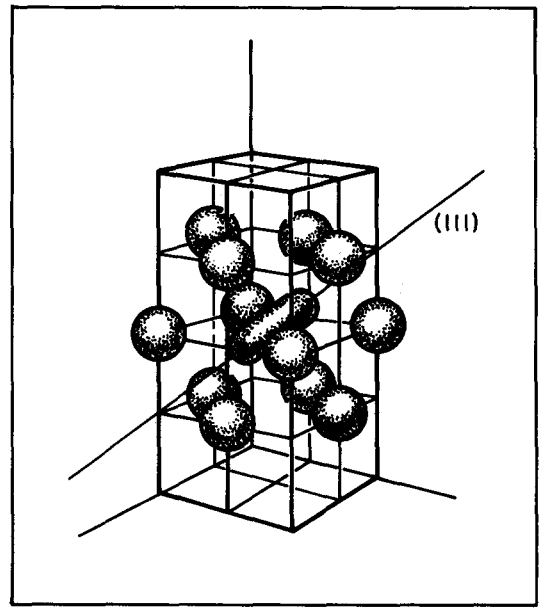


FIG. 8. The proposed orientation of HCN/Xe in site-1 along the $\langle 1, 1, 1\rangle$ axis. The H atom points between three nearest neighbors. The lattice probably distorts to accommodate the cylindrical molecule.

Molecular dynamics calculations by Nosé and Klein[23] predict an orientation of HCl in solid Ar by assuming additive pair potentials without considering the interaction of the HCl dipole with the induced Ar dipole. Since HCl rotates in rare gas matrices their calculations give a probability distribution for the vector directed along the Cl–H bond. They predict a preference for the $\langle 1\,1\,1\rangle$ direction for HCl in solid Argon, with a low probability of the $\langle 1\,0\,0\rangle$ orientation. Although HCN does not rotate in matrices it is, like HCl, a linear hydride and site-1 is probably the $\langle 1\,1\,1\rangle$ position (Fig. 8).

HCN in site-2 has a lower frequency C–H stretch and higher frequency bend. These shifts are in the same direction as those of the H-bonded HCN dimer. The $\langle 1\,1\,0\rangle$ direction with H pointed directly at a Xe atom seems to be a better candidate than $\langle 1\,1\,2\rangle$ pointed between two Xe atoms for site-2 (Fig. 9). The H-bonded van der Waals molecule type of interaction is more likely for the head-on $\langle 1\,1\,0\rangle$ orientation.

The differences in spectra in various rare gas hosts are consistent with this model. While the majority of the population in Xe is in site-2, in Kr (Fig. 1) the site-1 bands are more intense. Because Kr is less polarizable, the orienting force between site-2 HCN and the matrix is less strong. This reduces the site-2 population and results in a smaller red shift of the site-2 peak relative to site-1

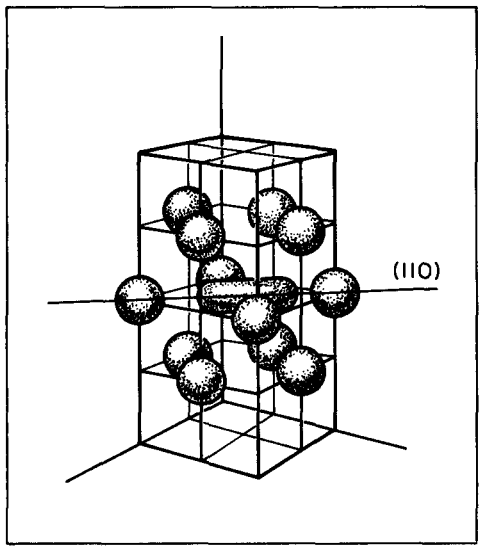


FIG. 9. The proposed orientation of HCN/Xe site-2 along the ⟨1, 1, 0⟩ axis. The H atom points directly at a Xe atom and the infrared bands of the C–H stretch and bend are shifted in the same direction as for the H-bonded dimer.

than in Xe. The $\nu_2$ degeneracy in Kr is not split sufficiently to produce two separate bands within 0.24 $cm^{-1}$ resolution and so the possibility that the two peaks are due to the two orientations which preserve the $\nu_2$ degeneracy must be admitted. In this case, site-2 would be the ⟨1 0 0⟩ orientation and the red shift of this peak would be attributed to an interaction with the second nearest neighbor, at which the H atom would be pointed. In an Ar matrix the combined effect of a smaller cage and a less polarizable host probably forces all of the HCN into the ⟨1 1 1⟩ orientation.

## IV. CONCLUSIONS

This spectroscopic study has provided fundamental and overtone frequencies and anharmonic constants for $HC^{14}N$ and $HC^{15}N$ in Ar, Kr, and Xe matrices, and for DCN in Xe. Multiple peaks were observed in the Kr and Xe matrices. Based on the changes in band intensity with annealing they were assigned to at least two sites. These assignments were supported by demonstrating that the same $\chi_{12}$ and $\chi_{23}$ anharmonicity constants can be used for both sites to reproduce the frequencies and relative intensities of the $\nu_1 + \nu_2$ and $\nu_2 + \nu_3$ combination bands.

In Xe the $\nu_2$ spectrum exhibits three peaks; this suggests that one of the trapping sites splits the $\nu_2$ degeneracy. A fit of the frequencies of the $\nu_2$ fundamental and first two overtones shows that this interpretation is more reasonable than a model with three sites, two of which overlap in frequency for some of the bands. A physical model of HCN in the ⟨1 1 1⟩ direction for site-1 and in the ⟨1 1 0⟩ direction for site-2 agrees nicely with all the Xe data. The shifts in the site-2 frequencies relative to site-1 are in the same direction as those of the hydrogen-bonded dimer: $\nu_2$ is blue shifted and $\nu_3$ is red shifted. This is reasonable for the ⟨1 1 0⟩ position in which the H atom is pointed directly at a rare gas atom. Furthermore, Figs. 8 and 9 show that while the bending degeneracy is preserved in the ⟨1 1 1⟩ direction, orthogonal bends of HCN in the ⟨1 1 0⟩ direction are not equivalent.

In Ar there is only one site; it is most probably the ⟨1 1 1⟩ orientation. The two sites in Kr are most probably the same as in Xe except that the splitting of the $\nu_2$ degeneracy for the ⟨1 1 0⟩ orientation is smaller.

These trapping sites are physically reasonable and are consistent with all the observed data. It is pleasing to have a complete and concrete physical explanation for the multiple peaks. This demonstrates that multiple peaked spectra can be a source of information on the structure of impurity trapping sites rather than an annoyance ascribed to mysterious multiple-site splittings.

## ACKNOWLEDGMENTS

We are grateful to the U.S. Army Research Office, Research Triangle Park, NC for support of this research. We thank Linda Young who recorded preliminary spectra of HCN and I. W. M. Smith who prepared the HCN sample.

[1] C. M. King and E. R. Nixon, J. Chem. Phys. **48,** 1685 (1968).
[2] J. Pacansky and G. V. Calder, J. Phys. Chem. **76,** 454 (1972).
[3] J. Pacansky and G. V. Calder, J. Mol. Struct. **14,** 363 (1972).
[4] B. Davies, A. McNeish, M. Poliakoff, M. Tranquille, and J. J. Turner, Chem. Phys. Lett. **52,** 477 (1977).
[5] B. Davies, A. McNeish, M. Poliakoff, and J. J. Turner, J. Am. Chem. Soc. **99,** 7573, (1977).
[6] G. C. Pimentel, M. O. Bulanin, and M. Van Thiel, J. Chem. Phys. **36,** 500 (1961).
[7] B. I. Swanson and L. H. Jones, J. Chem. Phys. **74,** 3205 (1981).
[8] L. H. Jones and B. I. Swanson, J. Chem. Phys. **74,** 3216 (1981).
[9] K. Kim and W. T. King, J. Chem. Phys. **71,** 1967 (1979).
[10] T. Nakagawa and Y. Morino, Bull. Chem. Soc. Jpn. **42,** 2212 (1969).
[11] I. W. M. Smith, J. Chem. Soc. Faraday Trans. 2 **77,** 2357 (1981).
[12] H. E. Hallam, in *Vibrational Spectroscopy of Trapped Species,* edited by H. E. Hallam (Wiley, New York, 1973), Chap. 3.
[13] C. H. Townes and A. L. Schawlow, *Microwave Spectroscopy* (Dover, New York, 1955), p. 30.
[14] Technical Manual, Nicolet 7199 FTIR.
[15] G. Herzberg, *Molecular Spectra and Molecular Structure* (Van Nostrand Reinhold, New York, 1979), Vol. II p. 211.
[16] G. Herzberg, *Molecular Spectra and Molecular Structure* (Van Nostrand Reinhold, New York), Vol. III p. 70.
[17] G. Herzberg, *Molecular Spectra and Molecular Structure* (Van Nostrand Reinhold, New York, 1979), Vol. II p. 229.
[18] G. Herzberg, *Molecular Spectra and Molecular Structure* (Van Nostrand Reinhold, New York, 1979), Vol. II p. 398.
[19] J. O. Hirschfelder, C. F. Curtiss, and R. B. Bird, *Molecular Theory of Gases and Liquids* (Wiley, New York, 1954), p. 1110.
[20] G. Herzberg, *Molecular Spectra and Molecular Structure* (Van Nostrand Reinhold, New York, 1979), Vol. II, p. 456.
[21] K. P. Huber and G. Herzberg, *Molecular Spectra and Molecular Structure* (Van Nostrand Reinhold, New York, 1979), Vol. IV, p. 420.
[22] H. E. Hallam and G. F. Scrimshaw, in *Vibrational Spectroscopy of Trapped Species,* edited by H. E. Hallam (Wiley, New York, 1973), Chap. 2.
[23] S. Nosé and M. L. Klein, Mol. Phys. **46,** 1063 (1982).